GLOBAL HIGH RESOLUTION CO_2 MONITORING USING SUPER RESOLUTION

Andrianirina Rakotoharisoa[1,2], Rossella Arcucci[1,2], Simone Cenci[3]
[1]Department of Earth Science & Engineering, Imperial College London, London, UK
[2]Data Science Institute, Imperial College London, London, UK
[3]Imperial College Business School, London, UK
{ar1619, r.arcucci, s.cenci}@imperial.ac.uk

ABSTRACT

Monitoring Greenhouse Gas (GHG) concentrations and emissions is essential to mitigate climate change. Thanks to the large amount of satellite data available, it is now possible to understand GHGs' behaviours at a broad scale. However, due to remote sensing devices technological limitations, the task of global high resolution (HR) monitoring remains an open problem. To avoid waiting for new missions and better data to be generated, it is therefore relevant to experiment with processing methods able to improve existing datasets. Our paper proposes to apply Super Resolution (SR), a Deep Learning (DL) approach commonly used in Computer Vision (CV), on global L3 satellite data. We produce a daily high resolution global CO_2 dataset that opens the door for globally consistent point source monitoring.

1 INTRODUCTION AND MOTIVATIONS

According to the sixth IPCC report, GHGs are responsible for an increase of the global surface temperature of over 1°since 1850-1900 (Core Writing Team et al.). Amongst GHGs, the report highlights the predominant role played by CO_2 and CH_4. Accurately understanding the emission process of GHGs can lead to more impactful decision making and actions to reduce global warming. Accordingly, emission datasets have been compiled by aggregating estimations and reports (Climate TRACE coalition, 2022; European Environment Agency, 2023). Besides, daily monitoring allows for emissions tracking (Nassar et al., 2021). A global HR daily GHG monitoring dataset could therefore help validate and complete these inventories. Unfortunately, remote sensing satellite imagery is either sparse and incomplete, as it will be generated following the swath of the satellite (Earth Science Data Systems, NASA, 2016), or possesses limited spatial or temporal resolution when processed to produce global maps. Studies have shown that machine learning methods can help overcome part of these limitations (He et al., 2022). The work described in this paper focuses on CO_2 monitoring and brings the following contributions:

- We apply SR to the Orbiting Carbon Observatory 2 (OCO-2) L3 dataset to generate HR global maps of column-averaged dry air mole fraction of atmospheric CO2 (XCO2). The framework can be transferred to other GHGs and is not specific to CO_2.
- We introduce a new HR dataset with a resolution of 0.03°*0.04°. This dataset offers the possibility to perform global XCO2 monitoring consistently.
- We show that our method does not introduce noise compared to the original Low Resolution (LR) dataset and offers a quantitative improvement in performance over alternative methods.

2 RELATED WORKS

Different methods have been used to produce global mapping datasets of XCO2. Statistical methods rely on interpolation to fill the gaps left by satellite-observed XCO2. Kriging interpolation and its variations compose the majority of the literature done following this approach (He et al., 2020; Zammit-Mangion et al., 2018; Bhattacharjee & Chen, 2020). Chemical Transport Model (CTM) simulations constitute a branch of statistical physics-informed methods to generate complete global data on XCO2, and in particular fluxes (Jacobson et al., 2023; Pillai & Neininger, 2012). The computational cost of these simulations unfortunately restricts the resolution of the global maps to coarse resolution. Other paradigms involve the fusion of multiple sensor's data in order to start with a more comprehensive covered area and therefore reduce the uncertainty of the generated maps (Wang et al., 2023). Finally, Machine Learning (ML) and DL-based methods are also found in the literature (He et al., 2022; Li et al., 2022).

3 METHODS

3.1 SUPER RESOLUTION

SR refers to the process of enhancing the resolution or quality of an image beyond its original level. This technique is commonly used in image processing and computer vision to improve the clarity and details of images. A higher-resolution version of an image is formed based on a LRinput (Tsai & Huang, 1984). When the input consists of only one image, it is referred to as Single Image Super Resolution (SISR) (Yang et al., 2019). As CV frameworks mostly rely on deep learning techniques, the current state of the art of SR models in remote sensing (RS) relies on neural networks (Wang et al., 2022b). The reconstructed output of a SR model presents features with greater detail than the LR input, thus enabling better analysis of the data. However, as SR is an inverse problem, different models will associate different SR images to the same input (Jo et al., 2021). In this work, the input is XCO2 data under matrix form. Converting this data to RGB images would require extra preprocessing steps, which would add noise to our input data. We therefore consider the task as a CV task where XCO2 maps are 1-channel images. Our model's architecture is a modified version of the framework from Haris et al. (2020), which was selected based on a benchmark on RS data done by Wang et al. (2022a). This model performs multiple up- and down-samplings iteratively to better extract the relation between LR and HR images. Convolutional and deconvolutional layers are associated to form the upsampling and downsampling blocks. It was initially developed to perform up to 8-times upsampling, so we adapted the kernel size, padding and striding. To avoid excessive memory usage and increase the training speed, we also modified the layers configuration to reduce the number of weights and applied the Distributed Data Parallel framework from PyTorch (Li et al., 2020). We have been able to increase the resolution 16-times, effectively bringing the XCO2 global maps' resolution close to 1km*1km, which is necessary to detect emission point sources.

4 DATASETS

4.1 TRAINING

As there is no HR XCO2 data for our model to learn from, we use the L3 products of the Land Surface Temperature (LST) dataset from MODIS (Wan et al., 2015) during the training phase. After downsampling the data, our model learns to reconstruct LST maps to its original resolution, which is approximately the same spatial resolution as our target resolution (see Table 1).

Table 1: Comparison of spatial resolution between L3 data from OCO-2 and MODIS satellites

	XCO2 L3 (OCO-2)	LST L3 (MODIS)
LR data (in degree)	0.5°*0.625°	0.8°*0.8°
HR data (in degree)	0.031°*0.039°(target)	0.05°*0.05°

4.2 Low resolution dataset

The OCO-2 and its successor OCO-3 are satellites from NASA. Their mission is to monitor CO_2 (Eldering et al., 2012) and they possess a radiometric resolution of the order of 1ppm. We use the L3 assimilated dataset (Weir et al., 2021) from OCO-2 as our LR dataset. This dataset consists of global maps of XCO2 at a resolution of 0.5°*0.625°. It is available at a daily or monthly temporal resolution, produced using NASA's modeling and data assimilation system.

4.3 Validation dataset

The Total Column Carbon Network (TCCON) (Wunch et al., 2011) is a family of ground sensors with sites located around the world that monitors column concentrations from CO_2,CH_4 (Parker et al., 2011), CO, and N_2O (Sha et al., 2020). To assess the accuracy of the SR XCO2 maps, we compare them with the latest version of TCCON data (Laughner et al., 2023). This data was obtained from the TCCON Data Archive hosted by CaltechDATA at https://tccondata.org.

5 Results and Discussion

We compare our results with pre-existing methods which also produce global data. Our benchmark consists of a dataset from Wang et al. (2023) obtained from the fusion of OCO-2 L2 data with the CAMS re-analysis dataset (Agusti-Panareda et al., 2022) and a HR dataset also derived from OCO-2 L3 data relying on bicubic interpolation as described in Xiang et al. (2022). These were selected for the quantitative quality of the produced data and their spatial and temporal availability.

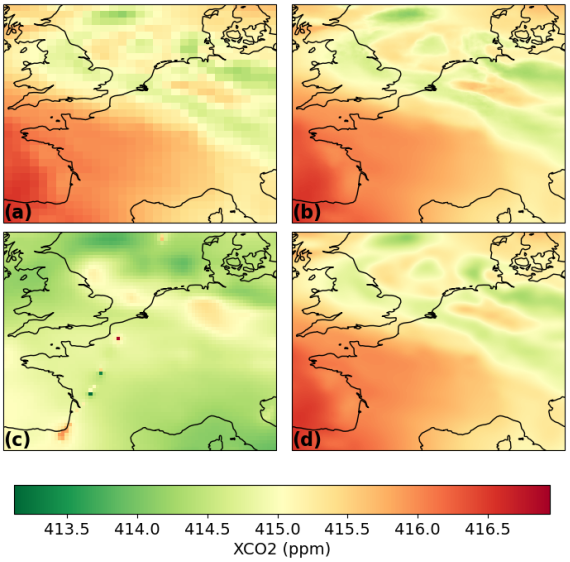

Figure 1: Visualisation of XCO2 over western Europe according to the four datasets used for this benchmark. From top left to bottom right: (a) LR dataset, (b) after SR (ours), (c) fusion dataset, (d) after bicubic interpolation. On this example, we observe a average bias difference between the LR and the fusion maps.

Figure 1 shows a visual comparison between our model and the benchmark methods for XCO2 data over western Europe. A smoothing effect is noticeable on the bicubic interpolation map over the North Sea (subfigure d) while more high-frequency details are created using our method (subfigure b).

Results displayed in Table 2 demonstrate that our SR model is able to significantly increase the resolution of the original LR dataset while improving on all the metrics. The comparison also holds when comparing the super resolved XCO2 maps with other methods. The fusion dataset presents on average a Root Mean Square Error (RMSE) well above 1ppm and a Mean Absolute Error (MAE) of 0.85ppm while our dataset lies at 0.92ppm and 0.70ppm respectively. Bicubic interpolation is a

close second on most metrics. Detailed results based on sensor location are presented in Appendix B and confirm that our method is more consistent spatially.

Table 2: Evaluation of the produced XCO2 data according to the benchmark

The best value for each metrics is highlighted. **LR** is the original OCO-2 L3 data, **BIC** is derived from bicubic interpolation, and **Fusion** is from Wang et al. (2023). Metrics are the average over every TCCON ground sensors location between 2015 and 2020

	SR (ours)	**LR**	**BIC**	**Fusion**
RMSE	**0.9180**	0.9441	0.9436	1.1196
R^2	**0.9673**	0.9654	0.9655	0.9514
MAE	**0.7027**	0.7182	0.7190	0.8505

To quantitatively assess the difference between SR using our model and using bicubic interpolation, we introduce an Improvement Ratio (IR) for each SR method. We define it as the following:

$$IR^{site} = \frac{N^{site}_{improved}}{N^{site}_{samples}} \tag{1}$$

where for each site, $N^{site}_{improved}$ represents the number of times where SR is closer to the ground truth and $N^{site}_{samples}$ represents the total number of samples for this site. A ratio of 1 (or 100%) indicates that the model always improves on the LR while a ratio of 0 indicates that the model always produces worse results.

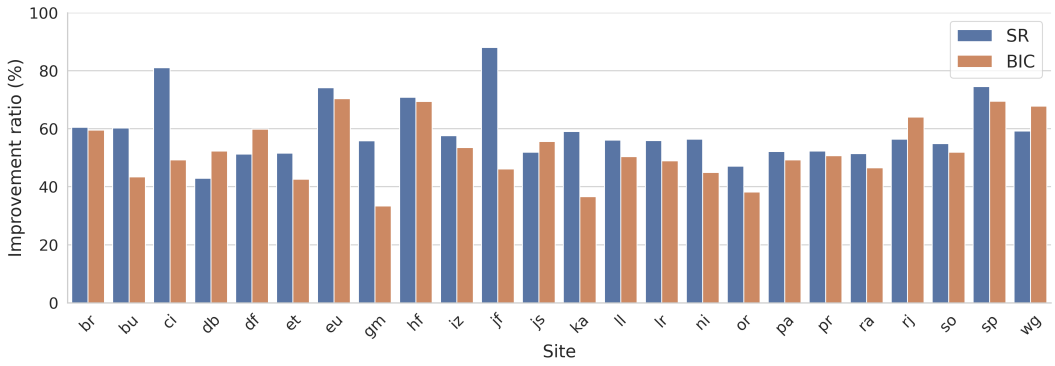

Figure 2: IR comparison between our model (blue) and bicubic (red) with available ground sensors data. The list of ground sensors abbreviations is presented in Appendix A.

Figure 2 shows that our model performs SR more consistently across the different sites, with the IR never going below 40% and only being worse than the bicubic one on 5 sites out of 24. This consistency is confirmed overall with our model producing an average IR of 57% against an average IR of 51% for bicubic SR.

5.1 Discussion

Our results show that our model outperforms other methods quantitatively. Furthermore, while they prove that it understands XCO2's behaviour better than statistical interpolation, we believe that more performance can be unlocked if we train the model on a physical variable closer to CO_2 than temperature. Additionally, including sparse data acquired from satellites could also lead to better results by guiding the model in its reconstruction of a SR map. Frameworks already exist to combine additional data with ML models (Buizza et al., 2022). Finally, Balashov et al. (2022) have indicated that XCH_4 L3 maps based on TROPOMI (Veefkind et al., 2012) data are currently being developed and will be released in the future. This will allow this work to be transferred to another GHG, increasing the relevance of our gas-agnostic framework.

6 CONCLUSION

In this paper we proposed a method to create a globally consistent daily HR XCO2 dataset. Our experiments have shown that our model is able to increase the resolution of the L3 maps produced by the OCO-2 to the order of 3km*4km while also improving concentration monitoring: our model is more robust spatially and temporally compared to other methods. This represents a good first attempt at applying SR to XCO2 fields and areas of improvement have been highlighted for future works. Moreover, the produced dataset provides the opportunity to study and quantify the impact of known sources on their surroundings or detect unreported point sources.

REFERENCES

Anna Agusti-Panareda, Jérôme Barré, Sébastien Massart, Antje Inness, Ilse Aben, Melanie Ades, Bianca C Baier, Gianpaolo Balsamo, Tobias Borsdorff, Nicolas Bousserez, et al. The CAMS greenhouse gas reanalysis from 2003 to 2020. *EGUsphere*, 2022:1–51, 2022.

Nikolay Balashov, Brad Weir, Lesley Ott, and Sourish Basu. Generating global CH4 NASA GEOS product by assimilating TROPOMI. In *AGU Fall Meeting*, number A15L-1387, 2022.

Shrutilipi Bhattacharjee and Jia Chen. Prediction of satellite-based column CO2 concentration by combining emission inventory and LULC information. *IEEE Transcations on Geoscience and Remote Sensing*, 58(12):8285–8300, 2020. doi: https://doi.org/10.1109/TGRS.2020.2985047. URL https://ieeexplore.ieee.org/abstract/document/9094001/. Query date: 2021-04-02 15:20:04.

Caterina Buizza, César Quilodrán Casas, Philip Nadler, Julian Mack, Stefano Marrone, Zainab Titus, Clémence Le Cornec, Evelyn Heylen, Tolga Dur, Luis Baca Ruiz, Claire Heaney, Julio Amador Díaz Lopez, K.S. Sesh Kumar, and Rossella Arcucci. Data learning: Integrating data assimilation and machine learning. *Journal of Computational Science*, 58:101525, 2022. ISSN 1877-7503. doi: https://doi.org/10.1016/j.jocs.2021.101525. URL https://www.sciencedirect.com/science/article/pii/S1877750321001861.

Climate TRACE coalition. Climate TRACE - Tracking Real-time Atmospheric Carbon Emissions. *Climate TRACE Emissions Inventory*, 2022. URL https://climatetrace.org/.

Core Writing Team, H. Lee, and J. Romero. Climate change 2023: synthesis report. Contribution of working groups I, II and III to the sixth assessment report of the intergovernmental panel on climate change. pp. 35–115. doi: 10.59327/IPCC/AR6-9789291691647.

Earth Science Data Systems, NASA. Data processing levels. 2016. URL https://www.earthdata.nasa.gov/engage/open-data-services-and-software/data-information-policy/data-levels.

Annmarie Eldering, Stacey Boland, Benjamin Solish, David Crisp, Peter Kahn, and Michael Gunson. High precision atmospheric CO2 measurements from space: The design and implementation of OCO-2. In *2012 IEEE aerospace conference*, pp. 1–10. IEEE, 2012.

European Environment Agency. National emissions reported to the UNFCCC and to the EU Greenhouse Gas Monitoring Mechanism. 2023. URL https://industry.eea.europa.eu/download.

Muhammad Haris, Greg Shakhnarovich, and Norimichi Ukita. Deep back-projectinetworks for single image super-resolution. *IEEE Transactions on Pattern Analysis and Machine Intelligence*, 43(12):4323–4337, 2020.

Changpei He, Mingrui Ji, Michael L Grieneisen, and Yu Zhan. A review of datasets and methods for deriving spatiotemporal distributions of atmospheric co2. *Journal of Environmental Management*, 322:116101, 2022.

Zhonghua He, Liping Lei, Yuhui Zhang, Mengya Sheng, Changjiang Wu, Liang Li, Zhao-Cheng Zeng, and Lisa R Welp. Spatio-temporal mapping of multi-satellite observed column atmospheric co2 using precision-weighted kriging method. *Remote Sensing*, 12(3):576, 2020.

A. R. Jacobson, K. N. Schuldt, and P. Tans. Carbontracker ct2022. *NOAA Global Monitoring Laboratory*, 2023. URL https://doi.org/10.25925/Z1GJ-3254.

Younghyun Jo, Seoung Wug Oh, Peter Vajda, and Seon Joo Kim. Tackling the ill-posedness of super-resolution through adaptive target generation. In *Proceedings of the IEEE/CVF Conference on Computer Vision and Pattern Recognition*, pp. 16236–16245, 2021.

Joshua L Laughner, Geoffrey C Toon, Joseph Mendonca, Christof Petri, Sébastien Roche, Debra Wunch, Jean-Francois Blavier, David WT Griffith, Pauli Heikkinen, Ralph F Keeling, et al. The total carbon column observing network's ggg2020 data version. *Earth System Science Data Discussions*, 2023:1–86, 2023.

Jie Li, Kun Jia, Xiangqin Wei, Mu Xia, Zhulin Chen, Yunjun Yao, Xiaotong Zhang, Haiying Jiang, Bo Yuan, Guofeng Tao, et al. High-spatiotemporal resolution mapping of spatiotemporally continuous atmospheric co2 concentrations over the global continent. *International Journal of Applied Earth Observation and Geoinformation*, 108:102743, 2022.

Shen Li, Yanli Zhao, Rohan Varma, Omkar Salpekar, Pieter Noordhuis, Teng Li, Adam Paszke, Jeff Smith, Brian Vaughan, Pritam Damania, et al. Pytorch distributed: Experiences on accelerating data parallel training. *arXiv preprint arXiv:2006.15704*, 2020.

Ray Nassar, Jon-Paul Mastrogiacomo, William Bateman-Hemphill, Callum McCracken, Cameron G MacDonald, Tim Hill, Christopher W O'Dell, Matthäus Kiel, and David Crisp. Advances in quantifying power plant co2 emissions with oco-2. *Remote Sensing of Environment*, 264:112579, 2021.

Robert Parker, Hartmut Boesch, Austin Cogan, Annemarie Fraser, Liang Feng, Paul I Palmer, Janina Messerschmidt, Nicholas Deutscher, David WT Griffith, Justus Notholt, et al. Methane observations from the greenhouse gases observing satellite: Comparison to ground-based tccon data and model calculations. *Geophysical Research Letters*, 38(15), 2011.

D Pillai and B Neininger. Comparing lagrangian and eulerian models for co 2 transport–a step towards bayesian inverse modeling using wrf/stilt-vprm. *Atmospheric Chemistry and Physics*, 12 (19):8979–8991, 2012.

Mahesh Kumar Sha, Martine De Mazière, Justus Notholt, Thomas Blumenstock, Huilin Chen, Angelika Dehn, David WT Griffith, Frank Hase, Pauli Heikkinen, Christian Hermans, et al. Intercomparison of low-and high-resolution infrared spectrometers for ground-based solar remote sensing measurements of total column concentrations of co 2, ch 4, and co. *Atmospheric Measurement Techniques*, 13(9):4791–4839, 2020.

Roger Y Tsai and Thomas S Huang. Multiframe image restoration and registration. *Multiframe image restoration and registration*, 1:317–339, 1984.

J Pepijn Veefkind, I Aben, K McMullan, H Förster, J De Vries, G Otter, Jacques Claas, HJ Eskes, JF De Haan, Q Kleipool, et al. Tropomi on the esa sentinel-5 precursor: A gmes mission for global observations of the atmospheric composition for climate, air quality and ozone layer applications. *Remote sensing of environment*, 120:70–83, 2012.

Z. Wan, S. Hook, and G. Hulley. Mod11c1 modis/terra land surface temperature/emissivity daily l3 global 0.05deg cmg v006 [data set]. 2015. URL `https://doi.org/10.5067/MODIS/MOD11C1.006`.

Peijuan Wang, Bulent Bayram, and Elif Sertel. A comprehensive review on deep learning based remote sensing image super-resolution methods. *Earth-Science Reviews*, pp. 104110, 2022a.

Yi Wang, Syed Muhammad Arsalan Bashir, Mahrukh Khan, Qudrat Ullah, Rui Wang, Yilin Song, Zhe Guo, and Yilong Niu. Remote sensing image super-resolution and object detection: Benchmark and state of the art. *Expert Systems with Applications*, pp. 116793, 2022b.

Yuan Wang, Qiangqiang Yuan, Tongwen Li, Yuanjian Yang, Siqin Zhou, and Liangpei Zhang. Seamless mapping of long-term (2010–2020) daily global xco 2 and xch 4 from the greenhouse gases observing satellite (gosat), orbiting carbon observatory 2 (oco-2), and cams global greenhouse gas reanalysis (cams-egg4) with a spatiotemporally self-supervised fusion method. *Earth System Science Data*, 15(8):3597–3622, 2023.

Brad Weir, Lesley Ott, and OCO-2 Science Team. OCO-2 GEOS level 3 daily, 0.5x0.625 assimilated CO2 v10r, 2021.

Debra Wunch, Geoffrey C Toon, Jean-François L Blavier, Rebecca A Washenfelder, Justus Notholt, Brian J Connor, David WT Griffith, Vanessa Sherlock, and Paul O Wennberg. The total carbon column observing network. *Philosophical Transactions of the Royal Society A: Mathematical, Physical and Engineering Sciences*, 369(1943):2087–2112, 2011.

Ru Xiang, Hui Yang, Zhaojin Yan, Abdallah M Mohamed Taha, Xiao Xu, and Teng Wu. Super-resolution reconstruction of gosat co2 products using bicubic interpolation. *Geocarto International*, 37(27):15187–15211, 2022.

Wenming Yang, Xuechen Zhang, Yapeng Tian, Wei Wang, Jing-Hao Xue, and Qingmin Liao. Deep learning for single image super-resolution: A brief review. *IEEE Transactions on Multimedia*, 21 (12):3106–3121, 2019. doi: 10.1109/TMM.2019.2919431.

Andrew Zammit-Mangion, Noel Cressie, and Clint Shumack. On statistical approaches to generate level 3 products from satellite remote sensing retrievals. *Remote Sensing*, 10(1):155, 2018.

ACRONYMS

CTM Chemical Transport Model
CV Computer Vision
DL Deep Learning
GHG Greenhouse Gas
HR high resolution
IR Improvement Ratio
LR Low Resolution
LST Land Surface Temperature
MAE Mean Absolute Error
ML Machine Learning
OCO-2 Orbiting Carbon Observatory 2
RS remote sensing
RMSE Root Mean Square Error
SISR Single Image Super Resolution
SR Super Resolution
TCCON Total Column Carbon Network
XCO2 column-averaged dry air mole fraction of atmospheric CO2

A TCCON VALIDATION SITES

Table 3: TCCON sites used in our experiments

Site (abbreviation)	Lat	Lon	Used Data Range
Bremen, Germany (br)	53.10N	8.85E	2015-2020
Burgos, Philippines (bu)	18.533N	120.650E	2017-2020
Caltech, USA (ci)	34.1362N	118.1269W	2015-2020
Darwin, Australia (db)	12.4246S	130.8917E	2015-2020
Edwards, USA (df)	34.958N	117.882W	2015-2020
East Trout Lake, Canada (et)	54.353738N	104.986667W	2016-2020
Eureka, Canada (eu)	80.05N	86.42W	2015-2020
Garmisch, Germany (gm)	47.476N	11.063E	2015-2020
Hefei, China (hf)	31.91N	117.17E	2015-2018
Izana, Tenerife (iz)	28.3N	16.5W	2015-2020
Jet Propulsion Lab, USA (jf)	34.958N	117.882W	2015-2018
Saga, Japan (js)	33.240962N	130.288239E	2015-2020
Karlsruhe, Germany (ka)	49.100N	8.439E	2015-2020
Lauder 02, New Zealand (ll)	45.038S	169.684E	2015-2018
Lauder 03, New Zealand (lr)	45.038S	169.684E	2018-2020
Nicosia, Cyprus (ni)	35.141N	33.381E	2019-2020
Orleans, France (or)	47.97N	2.113E	2015-2020
Park Falls, USA (pa)	45.945N	90.273E	2015-2020
Paris, France (pr)	48.846N	2.356E	2015-2020
Reunion Island, France (ra)	20.901S	55.485E	2015-2020
Rikubetsu, Japan (rj)	43.4567N	143.7661E	2015-2019
Sodankylä, Finland (so)	67.3668N	26.6310E	2015-2020
Ny Ålesund, Svalbard (sp)	78.9N	11.9E	2015-2020
Wollogong, Australia (wg)	34.406S	150.879E	2015-2020

B METRICS COMPARISON

Below are the detailed results of each metric: RMSE, R^2 coefficient and MAE. For each site, the best and second best methods are coloured in blue and red respectively. **LR** is the original OCO-2 L3 dataset, **BIC** is the dataset derived from bicubic interpolation and **Fusion** is the dataset from Wang et al. (2023).

Table 4: RMSE comparison to TCCON groundsensors

Site	SR (ours)	LR	BIC	Fusion
Eureka (eu)	1.3383	1.3586	1.3211	1.9763
Saga (js)	0.9605	0.9680	0.9359	1.2065
Izana (iz)	0.5865	0.5959	0.5928	0.6537
Caltech, Pasadena (ci)	1.2554	1.4637	1.4983	1.0894
Wollogong (wg)	0.7967	0.8212	0.7263	0.8271
Lauder 03 (lr)	0.6177	0.6244	0.6221	0.7700
Bremen (br)	0.9755	0.9960	0.9465	1.2262
Ny Ålesund (sp)	1.1519	1.1783	1.1217	1.5574
Lauder 02 (ll)	0.4979	0.5042	0.5064	0.6110
Park Falls (pa)	0.7756	0.7664	0.7784	1.0751
Hefei (hf)	1.3090	1.4783	1.2092	1.7435
Jet Propulsion Lab (jf)	1.1547	1.3822	1.3625	1.0809
Reunion Island (ra)	0.5984	0.5968	0.6022	0.7413
East Trout Lake (et)	0.7980	0.7971	0.8163	1.1310
Paris (pr)	1.3653	1.3867	1.3702	1.5325
Garmisch (gm)	0.9025	0.9114	1.0472	1.1098
Sodankylä (so)	0.9072	0.9149	0.9190	1.4612
Orleans (or)	1.1226	1.1175	1.1489	1.1886
Burgos (bu)	0.5196	0.5217	0.5557	0.7840
Edwards (df)	0.6880	0.6890	0.6482	1.0041
Rikubetsu (rj)	0.8888	0.9363	0.8300	1.3907
Karlsruhe (ka)	1.1230	1.1354	1.1852	1.3998
Nicosia (ni)	0.7677	0.7856	0.7864	1.0606
Darwin (db)	0.7107	0.6993	0.6969	0.9315

Table 5: R^2 coefficient comparison to TCCON groundsensors

Site	SR (ours)	LR	BIC	Fusion
Eureka (eu)	0.9414	0.9396	0.9429	0.8722
Saga (js)	0.9497	0.9489	0.9522	0.9206
Izana (iz)	0.9720	0.9711	0.9714	0.9653
Caltech, Pasadena (ci)	0.9344	0.9108	0.9065	0.9506
Wollogong (wg)	0.9695	0.9676	0.9746	0.9671
Lauder 03 (lr)	0.8866	0.8842	0.8850	0.8239
Bremen (br)	0.9656	0.9641	0.9676	0.9456
Ny Ålesund (sp)	0.9492	0.9469	0.9518	0.9072
Lauder 02 (ll)	0.9648	0.9639	0.9636	0.9470
Park Falls (pa)	0.9780	0.9785	0.9778	0.9577
Hefei (hf)	0.8371	0.7922	0.8610	0.7109
Jet Propulsion Lab (jf)	0.8003	0.7139	0.7220	0.8250
Reunion Island (ra)	0.9803	0.9804	0.9801	0.9698
East Trout Lake (et)	0.9677	0.9678	0.9662	0.9351
Paris (pr)	0.9169	0.9142	0.9163	0.8953
Garmisch (gm)	0.9641	0.9634	0.9517	0.9457
Sodankylä (so)	0.9747	0.9743	0.9741	0.9344
Orleans (or)	0.9499	0.9503	0.9475	0.9438
Burgos (bu)	0.9619	0.9616	0.9565	0.9133
Edwards (df)	0.9808	0.9807	0.9829	0.9591
Rikubetsu (rj)	0.9599	0.9554	0.9650	0.9017
Karlsruhe (ka)	0.9494	0.9482	0.9436	0.9213
Nicosia (ni)	0.8904	0.8852	0.8850	0.7908
Darwin (db)	0.9768	0.9775	0.9777	0.9601

Table 6: MAE comparison to TCCON groundsensors

Site	SR (ours)	LR	BIC	Fusion
Eureka (eu)	1.0063	1.0300	0.9877	1.5999
Saga (js)	0.7932	0.8003	0.7718	1.0232
Izana (iz)	0.4684	0.4778	0.4735	0.4869
Caltech, Pasadena (ci)	1.0030	1.1872	1.2032	0.8380
Wollogong (wg)	0.6091	0.6292	0.5511	0.6526
Lauder 03 (lr)	0.5136	0.5190	0.5194	0.6141
Bremen (br)	0.7651	0.7860	0.7410	0.9359
Ny Ålesund (sp)	0.9945	1.0191	0.9647	1.2495
Lauder 02 (ll)	0.3846	0.3903	0.3903	0.4704
Park Falls (pa)	0.6042	0.6036	0.6102	0.8507
Hefei (hf)	1.0729	1.2070	0.9880	1.4447
Jet Propulsion Lab (jf)	0.9821	1.1899	1.1811	0.8343
Reunion Island (ra)	0.4590	0.4584	0.4629	0.5769
East Trout Lake (et)	0.6309	0.6340	0.6478	0.9017
Paris (pr)	1.0909	1.0962	1.0935	1.2017
Garmisch (gm)	0.7116	0.7143	0.8455	0.8589
Sodankylä (so)	0.6997	0.7061	0.7071	1.1517
Orleans (or)	0.9229	0.9161	0.9503	0.9360
Burgos (bu)	0.4024	0.4097	0.4317	0.6334
Edwards (df)	0.5446	0.5423	0.5088	0.8139
Rikubetsu (rj)	0.6595	0.6974	0.6179	1.0873
Karlsruhe (ka)	0.9225	0.9346	0.9858	1.1060
Nicosia (ni)	0.6477	0.6666	0.6695	0.8737
Darwin (db)	0.5641	0.5552	0.5495	0.7219